Engineered Science

RESEARCH PAPER View Article Online

Fabrication and Characterization of Rose Bengal Sensitized Binary TiO_2-ZrO_2 Oxides Photo-electrode Based Dye-sensitized Solar Cell

M. A. Waghmare,[1,2] N. I. Beedri,[2] A. U. Ubale[1*] and H. M. Pathan[2]

Titanium oxide (TiO_2) electrode has been the most commonly used photo-electrode for the dye-sensitized solar cells (DSSCs). Several research groups have already reported that only TiO_2 layer is not yet ideal for electron transfer in the absence of space charge layer and also demonstrated the procedures for coating nanocrystalline semiconducting oxide films with a thin overcoat of a different semiconducting oxide with a higher conduction band energy level (E_C). Zirconium oxide (ZrO_2) is a suitable material for such overcoat because of its higher E_C. The binary TiO_2–ZrO_2 oxide photo-electrodes were prepared by doctor blading technique. The electrodes were annealed at 450 °C and then sensitized by Rose Bengal (RB) dye. The DSSC fabricated by binary TiO_2-ZrO_2 photo-electrode showed improved solar energy conversion efficiency than that of fabricated only by pure component of TiO_2.

Keywords: Zirconium Oxide; Titanium Oxide; Binary Oxides; Doctor Blade Technique; Dye-sensitized Solar Cell

Received 5 October 2018, **Accepted** 1 January 2019

DOI: 10.30919/es8d145

1. Introduction

DSSC based on nanocrystalline TiO_2 as a porous photo-electrode was firstly reported by O'regan and Gratzel.[1] As far as all solar energy devices are concerned, DSSCs have attained significant importance due to its low production cost as compared to other solar energy conversion devices. The power conversion efficiencies of TiO_2 based DSSCs considerably get influenced by its geometrical structures such as rutile, anatase and brookite.[2] In DSSCs, anatase (3.2 eV) TiO_2 nanopowder is commonly used to prepare photo-electrode films due to its higher Fermi-energy level and greater band gap energy as compared to rutile (3.0 eV).[3] Photovoltaic properties of DSSCs can be improved by modifying the properties of photo-electrode films. The charge transport and electrochemical properties of TiO_2 can be enhanced by introducing dopant such as W, Ta, Ni, Zr and Nb.[4-7] As far as these dopants are concerned, zirconium (Zr) has attained considerable interest for DSSC as it has the same valence shell structure $(n-1)\,d^2\,ns^2$ and same valence state as titanium (Ti).[6,8-10] There are many techniques reported to enhance the open circuit voltage (V_{OC}) of device. The V_{OC} of the device can be increased either by implementing bilayer technique[11-14] or by introducing changes in the structure of metal oxide semiconductor.[15,16] The bilayer technique is used to decrease recombination reactions. In this technique, a thin layer of another metal oxide having more negative conduction band edge (E_C) as compared to photo-electrode material is deposited on photo-electrode film. Another possible alternative to enhance V_{OC} is to increase E_C of the photo-electrode material by modifying its structure as V_{OC} depends upon the electron energy difference between the conduction band edge of photo-electrode and the redox potential level of electrolyte.[17] Kitiyanan *et al.*[18] have employed sol-gel method to prepare TiO_2-ZrO_2 (95 % TiO_2 + 5 % ZrO_2) mixed oxide system to increase efficiency of the cell. The cell parameters such as V_{OC} enhances to ~4 % , J_{SC} to ~11 % and η to ~17 % as compared to device prepared using TiO_2 photo-electrode film. Durr *et al.*[19] have revealed that for mixed Ti-Zr oxide system in DSSC, the V_{OC} of the device enhances with increase in Zr percentage. For higher Zr content, the device conversion efficiency decreases due to reduced electron injection. Menzies *et al.*[20] have investigated the photovoltaic performance of TiO_2 and ZrO_2-coated TiO_2 photo-electrodes calcined at 450 °C in a 2.45 GHz microwave furnace. The ZrO_2 shell-coating acts as an energy barrier between the photo-injected electrons in the conduction band of TiO_2 and the oxidized electrolyte species/dye molecules. The presence of ZrO_2 coating reduces the recombination rate of the injected photo-electrons into the conduction band of TiO_2 to either the oxidized electrolyte species or the oxidized dye molecules. The microwave calcined TiO_2 photo-electrode was found to be 2.4 % efficient whereas ZrO_2-coated TiO_2 showed efficiency up to 3.1 %. The presence of ZrO_2 shell showed enhancement in all the cell parameters such as J_{SC}, V_{OC} and FF. In DSSC, optical absorption can be enhanced by introducing light scattering layer forming double layer structure. Due to this light harvesting layer, the incident light remains confined within the photo-electrode which increases photocurrent density and efficiency of the device. Moradzaman *et al.*[21] have studied absorption effects, light

[1]*Nanostructured Thin Film Materials Laboratory, Department of Physics,Govt. Vidarbha Institute of Science and Humanities, Amravati - 444604, India*
[2]*Advanced Physics Laboratory, Department of Physics, Savitribai Phule Pune University, Pune - 411007, India*
***E-mail:** ashokuu@yahoo.com*

harvesting and light scattering in DSSC using Zr-doped TiO_2 photo-electrode. The double layer photo-electrode consisting of mixture 0.025 wt % carbon nanotubes (CNTs) with TiO_2 nanoparticles and 0.025 mol % Zr doped TiO_2 nanoparticles as an over layer and 0.025 mol % Zr doped TiO_2 nanoparticles as an under layer shows highest efficiency of 8.19 %. Sayyed *et al*.[22] have studied Rose Bengal (RB) dye-sensitized TiO_2–CeO_2 bilayer photo-electrodes for DSSC. They demonstrated that the introduction of CeO_2 layer reduces the recombination of photo-injected electrons with either the oxidized dye molecules or oxidized redox species which resulted into 38.10 % increase in J_{SC} and 66.67 % increase in V_{OC} as compared to the pure TiO_2 photo-electrode. Mohamed *et al*.[23] have revealed the influence of nanofibrous morphology and Zr-doping on the optical and electrical properties TiO_2. The DSSC fabricated using 1 % Zr-doped TiO_2 nanofibers showed highest photovoltaic efficiency of 4.51 % as compared to other doped samples (0.5, 1.5 and 2 % Zr-doped TiO_2 nanofibers). Beedri *et al*.[24] have enlightened the use of Nb_2O_5 as an energy barrier layer in N3 dye-sensitized ZnO/Nb_2O_5 photo-electrode based DSSC. They have noticed 10 % enhancement in the power conversion efficiency in ZnO/Nb_2O_5 photo-electrode due to increase in the lifetime of photo-injected electron as compared to the pure ZnO photo-electrode. They have also demonstrated the use of bilayer structure in N3 dye-sensitized TiO_2/Nb_2O_5 photo-electrode based DSSC to improve the overall power conversion efficiency.[25]

Anchoring group of dye sensitizer plays a vital role in deciding efficiency of the device. In the present work, Rose Bengal is used as a dye sensitizer. RB is a xanthene class of organic dye sensitizer which is widely used due to its noticeable merits such as low cost, moderate oxidation/reduction ability and high coefficient of absorption.[26-27]

The purpose of the present work is to investigate photovoltaic properties of DSSC with a porous TiO_2-ZrO_2 layer. ZrO_2 layer acts as an energy barrier layer between the oxidized redox couple/dye and photo-injected electrons to minimize recombination pathways.

2. Experimental section

2.1 Preparation of TiO_2 photo-electrodes

TiO_2 paste was prepared as per the literature method mentioned by Waghmare *et al*..[28] The TiO_2 paste was prepared by mixing 4 g TiO_2 nanopowder (SRL, APS. ~ 50 nm), 2 g ethyl cellulose (SRL), 1.8 ml terpineol (SRL), 5-6 drops of acetylacetone (SRL) and 20 ml ethanol (SRL). The TiO_2 paste was uniformly spread over the area of 0.6 cm x 0.4 cm (0.24 cm^2) on the FTO glass by doctor blade technique. The TiO_2 photo-electrode films were annealed at 450 °C for 1 h.

2.2 Preparation of TiO_2- ZrO_2 photo-electrodes

ZrO_2 paste preparation was adopted from Waghmare *et al*..[28] The ZrO_2 paste was prepared by mixing 4 g ZrO_2 nanopowder (SRL, APS. ~ 45 nm), 2 g ethyl cellulose (SRL), 1.8 ml terpineol (SRL), 5-6 drops of acetylacetone (SRL) and 20 ml ethanol (SRL). The TiO_2–ZrO_2 photo-electrode films were prepared by spreading the ZrO_2 paste uniformly over the area of 0.6 cm x 0.4 cm (0.24 cm^2) on the preformed TiO_2 photo-electrode film by doctor blade technique. The TiO_2–ZrO_2 photo-electrode films were annealed at 450 °C for 1 h. The photo-electrodes were prepared with different over layers of ZrO_2 on TiO_2 films. All the samples are named as $TiZr_x$, where x is the number of over layers of ZrO_2 on TiO_2 films, e.g. $TiZr_1$ is one over layer of ZrO_2 deposited on TiO_2 film (see Table 1).

2.3 DSSC fabrication

The TiO_2-ZrO_2 photo-electrodes were kept in 0.5 mM Rose Bengal dye solution prepared in ethanol at room temperature for 24 h. Thin Pt coated FTO glass was used as a counter electrode. The counter electrode was then kept in contact with the TiO_2-ZrO_2 photo-electrode films. A spacer was inserted between the TiO_2-ZrO_2 photo-electrode and the counter electrode to prevent the direct contact between them. The redox electrolyte was consisting of a 0.5 M lithium iodide (LiI) solution, a 0. 05 M iodine (I_2) solution and a 0.5 M 4-tert-butylpyridine solution in acetonitrile. It was introduced between the gap of the photo-electrode film and the counter electrode.

2.4 Characterization

X–ray diffraction (XRD) of the photo-electrode films was performed for phase identification and crystallite size determination by X-ray diffractometer (XRD, Rigaku "D/B max-2400", λ = 1.54 Å). The surface morphological and elemental analyses of the photo-electrodes were carried out by scanning electron microscopy (SEM, JEOL-JSM 6360-A) and energy-dispersive X-ray spectroscopy (EDX), respectively. The UV- vis absorption spectra of Rose Bengal in ethanol and adsorbed on TiO_2-ZrO_2 photo-electrode films were measured by UV–vis spectrometer (JascoV-670) in the range 200–800 nm. Electrochemical impedance spectroscopic (EIS) analyses were carried out to study the electron transfer at the photo-electrode / electrolyte interface. The applied ac signal voltage is 0.01 V in the frequency range of 1 Hz–1 MHz. EIS performed using Potentiostat/ Galnostat (Ivium Soft: Vertex) under dark. The photovoltaic performance of the fabricated cells was studied under an illumination of Xenon lamp of ~ 72 mW/cm^2 intensity using kiethley source meter (2420).

3. Results and discussion

3.1 XRD investigations of the photo-electrodes

Fig. 1 illustrates the diffraction patterns of ZrO_2, TiO_2 and ZrO_2 coated TiO_2 photo-electrode films on FTO substrate. The diffraction peaks observed at 26.44°, 33.64°, 37.71°, 51.48°, 61.48° and 65.40° are corresponding to crystal planes of (110), (101), (200), (211), (310) and (301), respectively can be ascribed to FTO [JCPDS card No. 46-1088]. The diffraction peaks of ZrO_2 can be attributed to monoclinic ZrO_2 [JCPDS card No. 37-1484] at 2θ values of 24.14°, 24.55°, 28.27°, 31.56°, 34.25°, 35.41°, 40.84°, 49.35°, 50.23°, 54.14° and 55.47° corresponding to the crystal planes of (110), (011), (-111), (111), (200), (002), (-112), (220), (022), (003) and (310) respectively (see Fig. 1a and Table 2). The crystallite size of the ZrO_2 nanopowder was calculated according to the Scherrer formula[29] along the most intense peak (-111). The crystallite

Table 1 Characteristics of fabricated DSSCs prepared with different over layers of ZrO_2 on TiO_2 photo-electrode films.

Cell	Number of over layers of ZrO_2
$TiZr_1$	1
$TiZr_2$	2
$TiZr_3$	3

Table 2 Comparison of observed XRD data of commercial ZrO_2 nanopowder with the JCPDS data. (JCPDS 37-1484)

Sample	Standard Values		Observed Values		h	k	l
	2θ (deg.)	*d* (nm)	2θ (deg.)	*d* (nm)			
ZrO_2	24.048	0.3696	24.139	0.3682	1	1	0
	24.441	0.3637	24.554	0.3621	0	1	1
	28.175	0.3163	28.269	0.3153	-1	1	1
	31.468	0.2839	31.561	0.2831	1	1	1
	34.160	0.2621	34.250	0.2614	2	0	0
	35.309	0.2538	35.414	0.2531	0	0	2
	40.725	0.2212	40.842	0.2206	-1	1	2
	49.266	0.1847	49.351	0.1844	2	2	0
	50.116	0.1818	50.231	0.1814	0	2	2
	54.104	0.1693	54.139	0.1692	0	0	3
	55.400	0.1656	55.469	0.1654	3	1	0

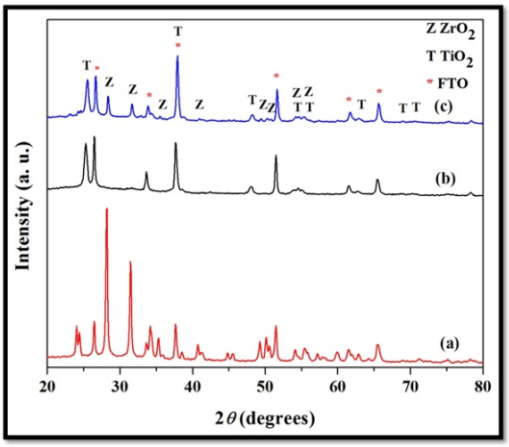

Fig. 1 XRD patterns of (a) ZrO_2, (b) TiO_2 and (c) ZrO_2 coated TiO_2 photo-electrodes on FTO substrate

size of the monoclinic ZrO_2 was 40 nm. Fig. 1b clearly demonstrates that the diffraction peaks of TiO_2 photo-electrode film can be attributed to anatase TiO_2 [JCPDS card No. 21-1272] at 2θ values of 25.32°, 37.73°, 48.07°, 55.07° and 62.68° , corresponding to the crystal planes of (101), (004), (200), (211) and (204), respectively.[23] The crystallite size of the TiO_2 sample was calculated according to the Scherrer formula along the most intense peak (101). The crystallite size of the anatase TiO_2 was 15.64 nm. The 2θ and (hkl) values of TiO_2 are summarized in Table 3. The ZrO_2 coated TiO_2 film shows diffraction peaks of anatase phase of TiO_2 as well as monoclinic phase of ZrO_2 structures. All the films samples (TiO_2, $TiZr_1$, $TiZr_2$ and $TiZr_3$) exhibit identical diffraction peaks of TiO_2 which confirm that anatase TiO_2 phase was retained in all photo-electrode films as it is required because of its photo-active nature.[18, 30]

3.2 SEM and EDX studies of the photo-electrodes

Fig. 2a-c presents SEM images of TiO_2, ZrO_2 and ZrO_2 coated TiO_2 photo-electrode films. The images show porous nature of the film samples. Porous films play a vital role in efficient light harvesting because light harvesting depends upon amount of dye adsorbed on the surface of photo-electrode film. Achieving efficient light harvesting, efficiency of the device can be enhanced. The compositional analyses were carried out using EDX technique. Fig. 3a-c displays the EDX patterns of TiO_2, ZrO_2 and ZrO_2 coated TiO_2 photo-electrode films. The existence of Ti, Zr and O was confirmed from EDX data.

3.3 Optical properties of the photo-electrodes

Fig. 4 shows the plot of $(\alpha h\upsilon)^2$ vs hυ of TiO_2 photo-electrode. The optical band gap of TiO_2 is estimated from the plot of $(\alpha h\upsilon)^2$ vs hυ. The band gap was found to be 3.22 eV. Many research groups have reported only an indirect band gap of 3.23 eV for anatase TiO_2. The obtained results are in good agreement with the previously reported results.[31-33] The optical band gap of ZrO_2 is calculated from the graph of $(\alpha h\upsilon)^2$ vs hυ (see Fig. 5). The band gap was found to be 5.14 eV. The obtained band gap value of ZrO_2 is consistent with the previously reported band gap values.[34-37] Absorption spectra of Rose Bengal dye is shown in Fig. 6a. The absorption spectra generally exhibits two absorption peaks. The peaks are observed in the short wavelength region (258 nm) as well as in the long (554 nm) wavelength region. The absorption peak in the long wavelength region attributed to the intra-molecular electron transfer within the highest occupied molecular orbital energy level (HOMO) to the lowest unoccupied molecular orbital (LUMO) energy level while the peak in the short wavelength region could be assigned to π to π^* electron transition.[38, 39] It is well known that the absorption of TiO_2 is limited to ultraviolet region (Fig. 6b) whereas the absorption of RB sensitized TiO_2 (Fig. 6c) and RB sensitized ZrO_2 coated TiO_2 (Fig. 6d) is extended to visible region (400 nm–600 nm).

Table 3 Comparison of observed XRD data of TiO_2 nanopowder with the JCPDS data. (JCPDS 21-1272)

Sample	Standard Values		Observed Values		h	k	l
	2θ (deg.)	*d* (nm)	2θ (deg.)	*d* (nm)			
TiO_2	25.281	0.3519	25.237	0.3525	1	0	1
	37.800	0.2377	37.765	0.2379	0	0	4
	48.049	0.1891	47.958	0.1895	2	0	0
	53.890	0.1699	53.903	0.1699	1	0	5
	55.060	0.1666	55.048	0.1666	2	1	1
	62.688	0.1480	62.632	0.1481	2	0	4
	68.760	0.1364	68.823	0.1362	1	1	6
	70.309	0.1337	70.293	0.1338	2	2	0
	75.029	0.1264	75.180	0.1262	2	1	5

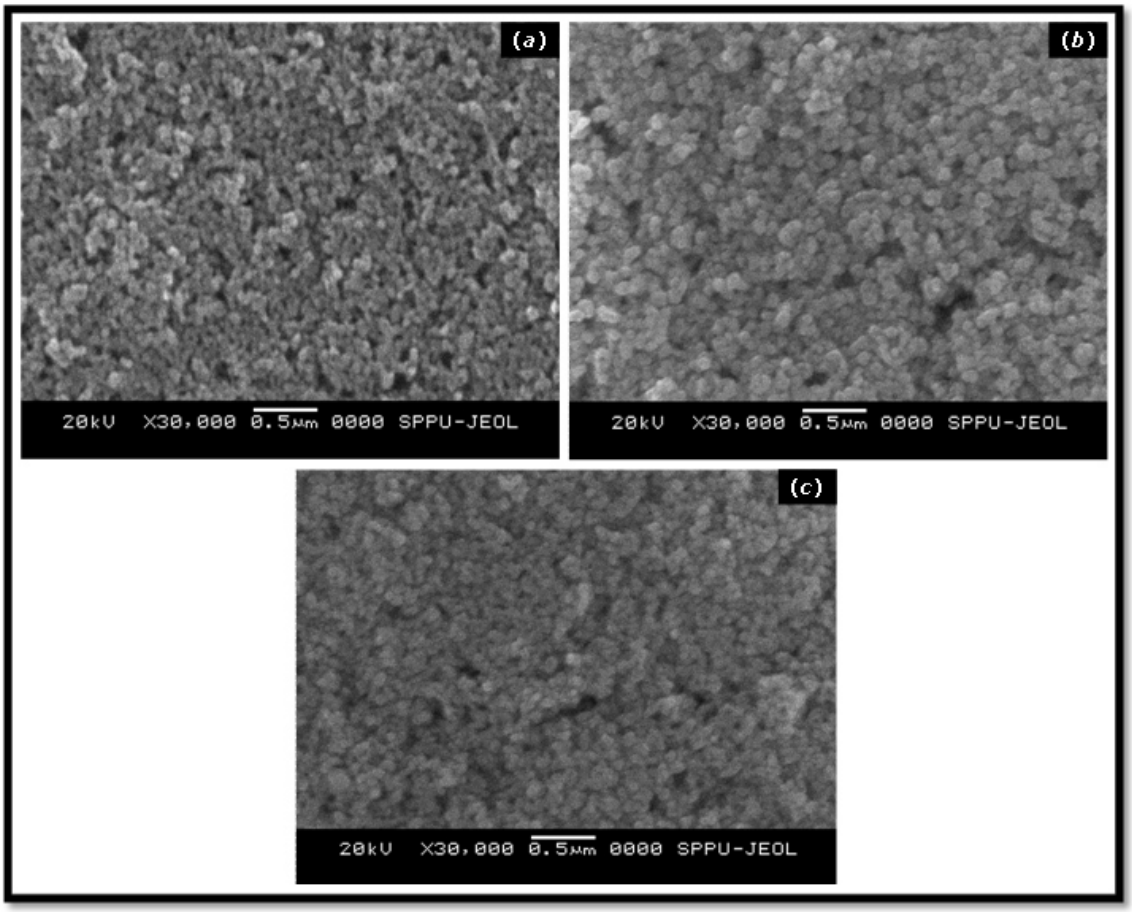

Fig. 2 SEM images of (a) TiO_2, (b) ZrO_2 and (c) ZrO_2 coated TiO_2 photo-electrode films.

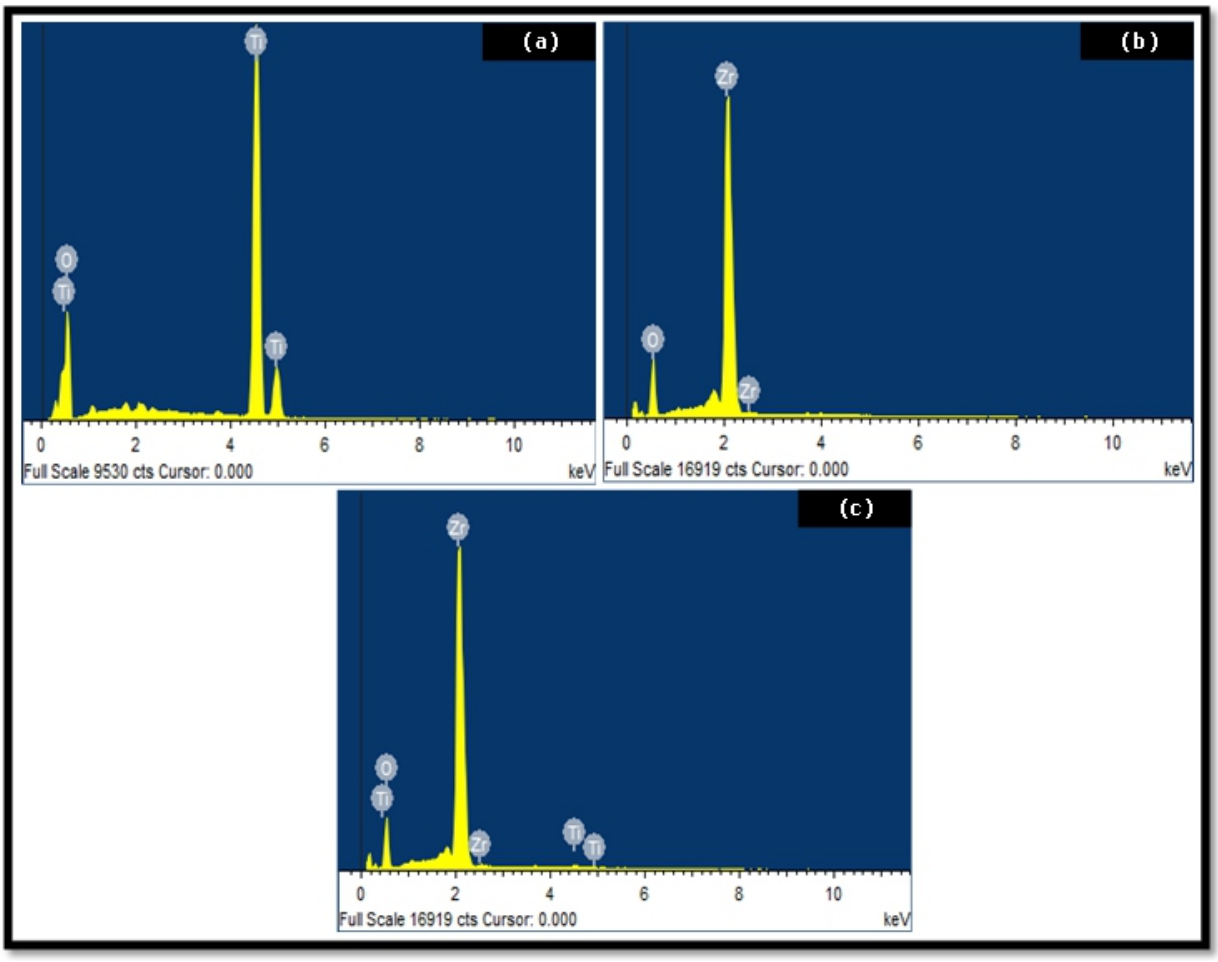

Fig. 3 EDX measurements of (a) TiO_2, (b) ZrO_2 and (c) ZrO_2 coated TiO_2 photo-electrode films.

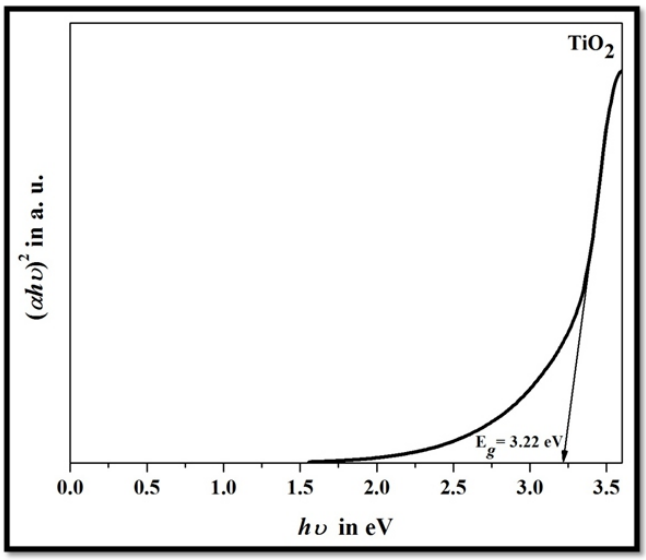

Fig. 4 Plot of $(\alpha h\upsilon)^2$ vs $h\upsilon$ of TiO_2 photo-electrode film.

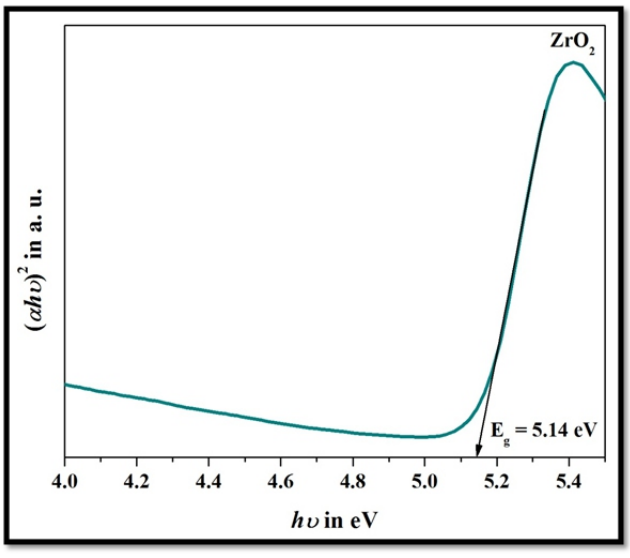

Fig. 5 Plot of $(\alpha h\upsilon)^2$ vs $h\upsilon$ of ZrO_2 photo-electrode film.

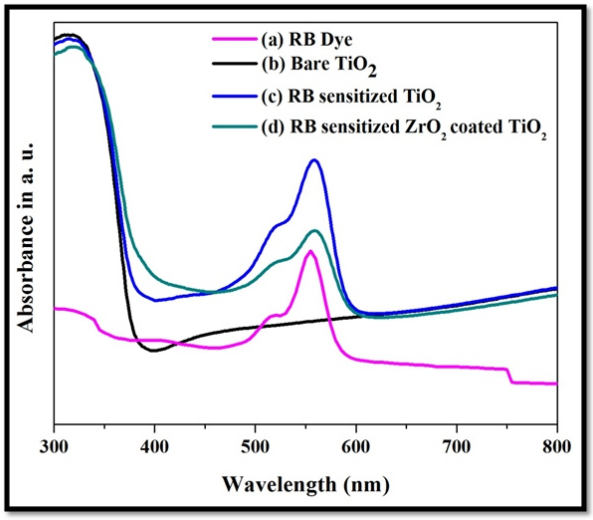

Fig. 6 UV-vis spectra of (a) RB dye, (b) bare TiO_2 photo-electrode, (c) RB sensitized TiO_2 and (d) RB sensitized ZrO_2 coated TiO_2 photo-electrodes.

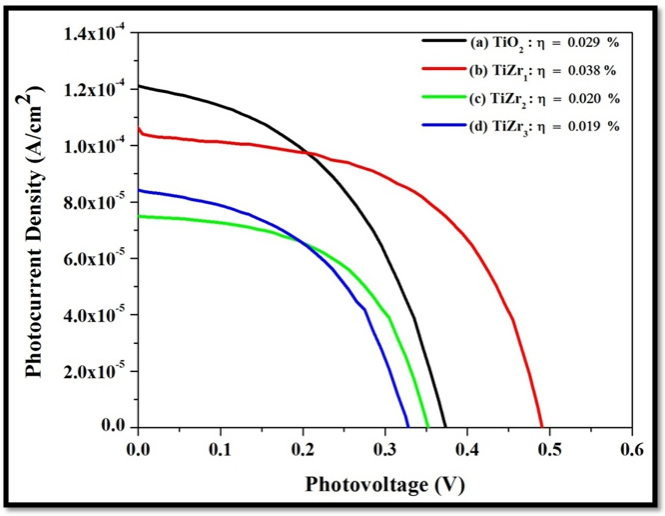

Fig. 7 J/V characteristics of DSSCs fabricated using Rose Bengal sensitized (a) TiO_2, (b) $TiZr_1$, (c) $TiZr_2$ and (d) $TiZr_3$ films. The data is obtained for the films of areas 0.24 cm^2 and under AM 1.5 simulated sunlight, ~72 mW /cm^2.

Table 4 Photovoltaic parameters of DSSCs fabricated using Rose Bengal sensitized (a) TiO_2 (b) $TiZr_1$ (c) $TiZr_2$ and (d) $TiZr_3$ films.

Photo-electrode	V_{OC} (V)	J_{SC} (mA/cm^2)	FF	η (%)
TiO_2	0.37	0.121	0.47	0.029
$TiZr_1$	0.4 9	0. 106	0.5 3	0.038
$TiZr_2$	0.35	0.075	0.54	0.020
$TiZr_3$	0.33	0.084	0.48	0.019

3.4 Photo-electrochemical characterization

Fig. 7 shows photovoltaic properties of Rose Bengal-sensitized TiO_2, $TiZr_1$, $TiZr_2$ and $TiZr_3$ photo-electrode films under light intensity of ~72 mW/cm^2. The photovoltaic properties of Rose Bengal-sensitized TiO_2, $TiZr_1$, $TiZr_2$ and $TiZr_3$ photo-electrode films prepared from commercial nanopowder by doctor blade technique are listed in Table 4. The J_{SC} was 0.121 mA/cm^2 for TiO_2, 0.106 mA/cm^2 for $TiZr_1$, 0.075 mA/cm^2 for $TiZr_2$, 0.084 mA/cm^2 for $TiZr_3$. For TiO_2, $TiZr_1$, $TiZr_2$ and $TiZr_3$, the V_{OC} was 0.37 V, 0.49 V, 0.35 V and 0.33 V, respectively. A large J_{SC} was observed for TiO_2 photo-electrode but V_{OC} was less as compared to $TiZr_1$. The power conversion efficiency for $TiZr_1$ was 0.038 % while it was 0.029% for TiO_2, 0.020% for $TiZr_2$ and 0.019 % for $TiZr_3$. It was noticed that the device fabricated with $TiZr_1$ photo-electrode film performed better as compared to other photo-electrodes. The ZrO_2 layer on TiO_2 photo-electrode film increases the V_{OC} by 32.43 % as compared to pure TiO_2. It was well reported that the interfacial electron recombination reactions decide V_{OC} of the device. The V_{OC} can be increased if the electron recombination reactions are minimized.[40] The implementation of ZrO_2 as an energy barrier layer between the TiO_2 photo-electrode and electrolyte reduces the back electron transfer from CB of TiO_2 to I_3^- in the electrolyte or to dye, thus improves V_{OC}.[41] The overall device efficiency shows a large enhancement 31.03 % as compared to pure TiO_2 photo-electrode film. The open circuit voltage decreases with increase in number of over layers of ZrO_2 which decreases the photovoltaic efficiency (0.020 % for $TiZr_2$ and 0.019 % for $TiZr_3$). It was observed that the introduction of ZrO_2 over layer decreases the recombination pathways which enhances the device performance but it was also noticed that with increase in number of over layers, the electron tunneling path length through the ZrO_2 barrier layer into TiO_2 photo-electrode film increases which decreases the overall device performance for $TiZr_2$ and $TiZr_3$.[42] If ZrO_2 film thickness is increased then the photo-excited electrons will not readily get injected into the conduction band of TiO_2 photo-electrode film and they may recombine with the oxidized dye or electrolyte. These recombination reactions decrease the photo-current density.[30] Hence, for thicker ZrO_2 over layers, a significant decrease in the photovoltaic parameters was observed.[43]

In DSSCs, the electrochemical impedance spectroscopy (EIS) is a powerful technique to explore the charge transfer dynamics at the film interfaces.[44] Fig. 8 shows the Nyquist plots recorded in dark under forward bias (0.7 V) condition of the fabricated DSSCs using TiO_2 and different over layers of ZrO_2 on TiO_2 photo-electrode films ($TiZr_1$, $TiZr_2$ and $TiZr_3$). As observed in Fig. 8 the Nyquist plots exhibit two semicircles, the first semicircle explains the charge-transfer resistance at counter electrode/electrolyte and the second circle reveals charge recombination resistance at the TiO_2/electrolyte interface (R_{rec}).[45] The rate

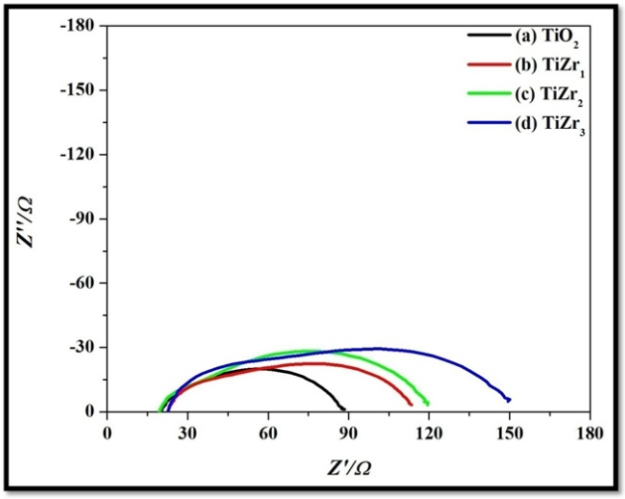

Fig. 8 Nyquist plots observed for the DSSCs fabricated using Rose Bengal sensitized (a) TiO_2 (b) $TiZr_1$ (c) $TiZr_2$ and (d) $TiZr_3$ films.

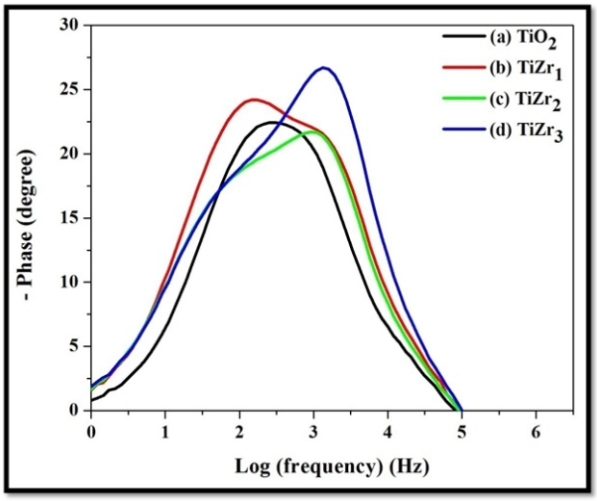

Fig. 9 Bode phase plots observed for the DSSCs fabricated using Rose Bengal sensitized (a) TiO_2 (b) $TiZr_1$ (c) $TiZr_2$ and (d) $TiZr_3$ films.

Table 5 EIS parameters of DSSCs fabricated using Rose Bengal sensitized (a) TiO_2 (b) $TiZr_1$ (c) $TiZr_2$ and (d) $TiZr_3$ films.

Photo-electrode	R_s (Ω)	R_{rec} (Ω cm^2)	Peak Phase (°)	f_{max} (Hz)	τ_e (ms)
TiO_2	18.2	64.6	22.4	251	0.63
$TiZr_1$	20.5	92.9	24.2	174	0.91
$TiZr_2$	17.2	102.2	21.7	912	0.17
$TiZr_3$	20.9	128.8	26.7	1320	0.12

at which the charge transfer takes place depends upon the radius of semicircles. As listed in the Table 5, the R_{rec} value of the TiO_2, $TiZr_1$, $TiZr_2$ and $TiZr_3$ photo-electrode films were 64.6 , 92.9 , 102.2 and 128.8 , respectively. The TiO_2 photo-electrode film shows low charge recombination resistance as compared to other photo-electrode films. The implementation of ZrO_2 over layers on TiO_2 photo-electrode films increases the R_{rec} values. The introduction of ZrO_2 over layer plays a decisive role in minimizing charge recombination losses as it acts as a barrier layer between the TiO_2 and dye or redox electrolyte. Fig. 9 displays Bode phase plot of the fabricated DSSCs using TiO_2 and different over layers of ZrO_2 on TiO_2 photo-electrode films. The electron lifetime (τ_e) in TiO_2, $TiZr_1$, $TiZr_2$ and $TiZr_3$ photo-electrode films can be calculated using the equation: $\tau_e = 1/2\pi f_{max}$, where f_{max} is the maximum peak frequency. As listed in Table 5, the f_{max} values of TiO_2, $TiZr_1$, $TiZr_2$, and $TiZr_3$ are 251, 174, 912 and 1320 Hz and the electron life time values are estimated to be 0.63, 0.91, 0.17 and 0.12 ms. The f_{max} values exhibit a decrease from TiO_2 to $TiZr_1$. The electron life time in $TiZr_1$ was prolonged from 0.63 to 0.91 ms. The prolonged electron life time indicates minimization in charge recombination losses which enhances the overall power conversion efficiency of the device. The obtained results are in good agreement with the J/V analysis data.

4. Conclusions

We have demonstrated a novel approach to improve the efficiency of dye-sensitized solar cell. We have proven that the introduction of ZrO_2 layer over TiO_2 photo-electrode film improves the photovoltaic parameters significantly which leads to increase in the overall power conversion efficiency.

Acknowledgement

Authors are thankful to Board of College and University Development (BCUD), Savitribai Phule Pune University, Pune for financial support under the project.

References

1. B. O'regan and M. Grätzel, *Nature*, 1991, **353**, 737-740.
2. A. Zaleska, *Recent Patents Eng.*, 2008, **2**, 157-164.
3. A. K. Chandiran, F. Sauvage, M. Casas-Cabanas, P. Comte, S. Zakeeruddin and M. Graetzel, *J. Phys. Chem. C*, 2010, **114**, 15849–15856.
4. H. Liu, J. Tang, I. J. Kramer, R. Debnath, G. I. Koleilat, X. Wang, A. Fisher, R. Li, L. Brzozowski, L. Levina and E. H. Sargent, *Adv. Mater.*, 2011, **23**, 3832–3837.
5. X. Zhang, F. Liu, Q. L. Huang, G. Zhou and Z. S. Wang, *J. Phys. Chem. C*, 2011, **115**, 12665–12671.
6. J. Y. Park, K. H. Lee, B. S. Kim, C. S. Kim, S. E. Lee, K. Okuyama, H. D. Jang and T. O. Kim, *RSC Advances*, 2014, **4**, 9946-9952.
7. R. L. Z. Hoye, K. P. Musselman and J. L. Macmanus-Driscoll, *APL Mater.*, 2013, **1**, 060701-060711.
8. P. S. Archana, A. Gupta, M. M. Yusoff and R. Jose, *Appl. Phys. Lett.*, 2014,

105, 153901-153905.
9. S. Kim and M. Kang, *Bull. Korean Chem. Soc.*, 2011, **32**, 3317–3322.
10. J. Wang, E. M. Jin, J. Y. Park, W. L. Wang, X. G. Zhao and H. B. Gu, *Nanoscale Res. Lett.*, 2012, **7**, 1–4.
11. Z. S. Wang, C. H. Huang, Y. Y. Huang, Y. J. Hou, P. H. Xie, B. W. Zhang and H. M. Cheng*, Chem. Mater.*, 2001, **13**, 678-682.
12. A. Kay and M. Grätzel, *Chem. Mater.*, 2002, **14**, 2930-2935.
13. S. Chappel, S. G. Chen and A. Zaban, *Langmuir*, 2002, **18**, 3336-3342.
14. E. Palomares, J. N. Clifford, S. A. Haque, T. Lutz and J. R. Durrant, *Chem. Commun.*, 2002, 1464-1465.
15. M. Adachi, I. Okada, S. Ngamsinlapasathian, Y. Murata and S. Yoshikawa, *Electrochemistry*, 2002, **70**, 449-452.
16. S. Uchida, R. Chiba, M. Tomiha, N. Masaki and M. Shirai, *Electrochemistry*, 2002, **70**, 418-420.
17. D. Cahen, G. Hodes, M. Graetzel, J. F. Guillemoles and I. Riess, *J. Phys. Chem. B*, 2000, **104**, 2053-2059.
18. A. Kitiyanan, S. Pavasupree, T. Kato, Y. Suzuki and S. Yoshikawa, *As. J. Energy Env.*, 2005, **6**, 165-174.
19. M. Dürr, S. Rosselli, A. Yasuda and G. Nelles, *J. Phys. Chem. B*, 2006, **110**, 21899-21902.
20. D. B. Menzies, Q. Dai, Y. B. Cheng, G. P. Simon and L. Spiccia, *C. R. Chimie*, 2006, **9**, 713-716.
21. M. Moradzaman, M. R. Mohammadi and H. Nourizadeh, *Mater. Sci. Semicond. Process.*, 2015, **40**, 383-390.
22. S. A. Sayyed, N. I. Beedri, V. S. Kadam and H. M. Pathan, *Appl. Nanosci.*, 2016, **6**, 875-881.
23. I. M. Mohamed, V. D. Dao, N. A. Barakat, A. S. Yasin, A. Yousef and H. S. Choi, *J. Colloid Interf. Sci.*, 2016, **476**, 9-19.
24. N. I. Beedri, P. K. Baviskar, A. T. Supekar, Inamuddin, S. R. Jadkar and H. M. Pathan, *Int. J. Mod. Phys. B*, 2018, **32**, 1840046.
25. N. I. Beedri, P. K. Baviskar, V. P. Bhalekar, C. V. Jagtap, A. M. Asiri, S. R. Jadkar and H. M. Pathan, *Phys. Status. Solidi A*, 2018, **215**, 1800236.
26. K. Hara , T. Sato , R. Katoh , A. Furube , Y. Ohga , A. Shinpo , S. Suga , K. Sayama , H. Sugihara and H. Arakawa , *J. Phys. Chem. B,* 2003, **107**, 597-606.
27. B. Pradhan, S. Batabyal and A. Pal, *Sol. Energy Mater. Sol. Cells,* 2007, **91**, 769-773.
28. M. A. Waghmare, M. Naushad, H. M. Pathan and A. U. Ubale, *J. Solid State Electrochem.*, 2017, **21**, 2719-2723.
29. B. D. Cullity, *Elements of X-ray Diffraction*, *Addison-Wesley Publishing Company, Inc., London*, 1978, 99.
30. D. B. Menzies, R. Cervini, Y. B. Cheng, G. P. Simon and L. Spiccia, *J. Sol–Gel Sci. Technol.*, 2004, **32**, 363-366.
31. A. Welte, C. Waldauf, C. Brabec and P. Wellmann, *Thin Solid Films*, 2008, **516**, 7256-7259.
32. D. Monllor-Satoca, R. Gomez, M. González-Hidalgo and P. Salvador, *Catal. Today*, 2007, **129**, 247-255.
33. K. M. Reddy, S. V. Manorama and A. R. Reddy, *Mater. Chem. Phys.*, 2003, **78**, 239-245.
34. D. P. Thompson, A. M. Dickins and J. S. Thorp, *J. Mater. Sci.*, 1992, **27**, 2267-2271.
35. M. M. Rashad and H. M. Baioumy*, J. Mater. Process. Technol.*, 2008, **195**, 178-185.
36. F. Davar and M. R. Loghman-Estarki, *Ceram. Int.*, 2014, **40**, 8427-8433.
37. C. R. Chintaparty, *Optik*, 2016, **127**, 4889-4893.
38. S. P. Singh, M. S. Roy, K. J. Thomas, S. Balaiah, K. Bhanuprakash and G. D. Sharma, *J. Phys. Chem. C*, 2012, **116**, 5941-5950.
39. R. Schlaf, P. G. Schroeder, M. W. Nelson, B. A. Parkinson, C. D. Merritt, L. A. Crisafulli, H. Murata and Z. H. Kafafi, *Surf. Sci.*, 2000, **450**, 142-152.
40. G. Boschloo and A. Hagfeldt, *Acc. Chem. Res.*, 2009, **42**, 1819–1826.
41. B. Oregan, S. Scully and A. Mayer, *J. Phys. Chem. B*, 2005, **109**, 4616–4623.
42. S. G. Chen, S. Chappel, Y. Diamant and A. Zaban, *Chem. Mater.*, 2001, **13**, 4629-4634.
43. T. C. Li, M. S. Goes, F. Fabregat-Santiago, J. Bisquert, P. R. Bueno, C. Prasittichai, J. T. Hupp and T. J. Marks, *J. Phys. Chem. C*, 2009, **113**, 18385−18390.
44. Q. Wang, J. E. Moser and M. Gratzel, *J. Phys. Chem. B*, 2005, **109**, 14945-14953.
45. K. M. Lee, C. W. Hu, H. W. Chen and K. C. Ho, *Sol. Energy Mater. Sol. Cells*, 2008, **92**, 1628-1633.